Universal avalanche statistics and triggering close to failure in a mean-field model of rheological fracture

Jordi Baró* and Jörn Davidsen
Department of Physics and Astronomy University of Calgary, 2500 University Drive, NW Calgary, Alberta, Canada T2N 1N4

(Received 5 January 2018; published 29 March 2018)

The hypothesis of critical failure relates the presence of an ultimate stability point in the structural constitutive equation of materials to a divergence of characteristic scales in the microscopic dynamics responsible for deformation. Avalanche models involving critical failure have determined common universality classes for stick-slip processes and fracture. However, not all empirical failure processes exhibit the trademarks of criticality. The rheological properties of materials introduce dissipation, usually reproduced in conceptual models as a hardening of the coarse grained elements of the system. Here, we investigate the effects of transient hardening on (i) the activity rate and (ii) the statistical properties of avalanches. We find the explicit representation of transient hardening in the presence of generalized viscoelasticity and solve the corresponding mean-field model of fracture. In the quasistatic limit, the accelerated energy release is invariant with respect to rheology and the avalanche propagation can be reinterpreted in terms of a stochastic counting process. A single universality class can be defined from such analogy, and all statistical properties depend only on the distance to criticality. We also prove that interevent correlations emerge due to the hardening—even in the quasistatic limit—that can be interpreted as "aftershocks" and "foreshocks."

DOI: 10.1103/PhysRevE.97.033002

I. INTRODUCTION

The mechanical failure of natural or man-made structures due to the variations of the external loads or long exposure to extreme external conditions constitutes a common hazard of major concern in seismology and civil engineering. Experimental studies reveal that the mechanical deformation of crystalline structures [1,2], amorphous materials [3,4], and jammed granular (or fragile) matter [5,6] is highly affected by the inherent heterogeneity in the system [7] or some degree of disorder such as defects, dislocations, or inclusions. Hence, failure is difficult to forecast because of the sensitivity to the unknown internal details of the system. In micromechanical models of failure [8–21], the addition of disorder is able to arrest the internal micromechanical processes responsible for deformation in multiple metastable states, leading to stochastic avalanche dynamics [22]. The arrested energy is partially released during the mechanical avalanche as elastic waves that can be detected by means of seismographs and geophones at the geological scale [23,24], or by ultrasonic acoustic emission (AE) equipment [25,26] in laboratory controlled experiments (see, for example, [5,26–37]). Such elastic waves can be used as probes to assess the state of the system and develop reliable forecasting tools for structural health monitoring [38,39].

A. Accelerated seismic release and criticality

Mechanical failure appears as a consequence of weakening or yielding of the strain (ε_{ij}) stress (σ_{ij}) relation. The susceptibility of the strain to variations of the stress tensor—a parameter simplified in this work by a scalar variable or inverse modulus $G^{-1} = d\varepsilon/d\sigma$—increases as the material weakens. As a consequence, the energy released as elastic waves—trademark of the amount of deformation—also increases close to failure. This increased energy release has been claimed to be present in the vicinity of major earthquakes—or mainshocks—and it is usually referred to as accelerated moment or seismic release (AMR or ASR) in both seismology and AE experiments [30,40–43], although its validity in seismology is controversial [41,44,45], and rarely outscores linear models as a forecasting tool [46]. Several micromechanical models governed by quenched disorder justify the observation of ASR by the presence of a critical point matching failure [11,19,21,40,47–50]. Again, in the case of seismology, this hypothesis might be questionable [47,51,52]. In the presence of a critical point, close to criticality the distribution of avalanche energies (E) can be described by a generalized homogeneous function:

$$D(E; f)dE = E^{-\epsilon}\mathcal{D}(Ef^{\beta})dE = f^{\beta\epsilon}\tilde{\mathcal{D}}(Ef^{\beta})dE, \quad (1)$$

with a scaling function $\mathcal{D}$ that depends only on the combined argument Ef^{β}. Here, f accounts for the distance to failure and is defined in terms of the time remaining to reach the failure point $f = 1 - t/t_f$. In critical failure models, the observed ASR is a natural consequence of the increase of the mean event energy: If the activity rate is constant, the energy rate $\frac{dE(f)}{df}$ will be proportional to $\langle E(f)\rangle \sim f^{(\varepsilon-2)\beta} \sim (t - t_f)^{(\varepsilon-2)\beta}$. Although widely accepted [19,45] this explanation is insufficient in the presence of nonconservative processes, which are known to play an important role in rock fracture [7]. The addition of dissipation introduce length scales and can prevent criticality [53], as specifically shown in branching processes [54], stick-slip models [55], and depinning interface models [56].

*jordi.barourbea@ucalgary.ca

Instead of, or in addition to, criticality, almost all experimental studies show an increase in the number of events coinciding with failure [27,37,57,58] and/or large events [34–36], typically denoted as the inverse Omori law of foreshocks [59,60]. Such a behavior at the failure point is not reproduced by standard micromechanical models and the provided analytical solutions implicitly consider constant activity rates [12,61]. As shown experimentally [41,62], ASR can simply be a consequence of this increase in the number of events alone.

B. About this work

In the present paper we argue that the same processes responsible for the observed history-dependent activity [26,34–37], namely relaxation mechanisms [9,55,56,63,64–70] often related to event-event triggering [71–74], can explain ASR as peaks of activity, even in the absence of critical failure or any temporal variation in the statistical properties of the AE events. We show that the emergence of relaxation processes and the associated temporal correlations can be a direct consequence of dissipation as modeled by transient hardening. We mathematically explain the link between aftershocks, foreshocks, critical failure, and accelerated seismic release at a fundamental level in a solvable model of fracture with generalized viscoelasticity.

The starting point of our study is a prototypical model of fracture: the democratic fiber bundle model (Sec. II A). Incorporating experimental findings, we propose a variation of the model with a physically based transient effect, which we denote as the generalized viscoelastic democratic fiber bundle model (Sec. II C), which is able to generate relaxation processes and triggering (Sec. II G). We prove analytically that this model can be approximated to the more simple and general concept of transient hardening (Sec. II F). Our goal is to characterize analytically the effect of transient hardening on the propagation and statistics of micromechanical avalanches. We derive the mean-field (MF) solution of the transient hardening model in the thermodynamic limit (Sec. III). In the process, we reinterpret the model as a fundamental stochastic problem. We find that a unified universality class (UC) for fracture models can be derived from this model, which is distinct in its initial formulation from the MF model of slip avalanches [12] and critical branching processes [75]. In the presence of transient hardening, the critical point is never reached. The magnitude of transient hardening and the distance to the failure point are combined in a single parameter—the distance to criticality—that fully determines the characteristic scales of avalanche statistics. We test our analytical results with numerical simulations of the viscoelastic model. The numerical findings for the standard viscoelastic case are presented in Sec. IV. The temporal evolution of the distance to criticality during the failure process depends on the driving mechanism (Sec. IV A). The function of the stochastic sampling and the magnitude of the hardening completely define the avalanche size distribution (Sec. IV B), the evolution of the activity rate, and the seismic release of the process leading to failure (Sec. IV C). We observe Omori-like behavior—typically associated with triggering and aftershocks [59,71]—with self-consistent specific exponents (Sec. IV D). We comment on the implications for the experimental observations and present some concluding remarks in Sec. V.

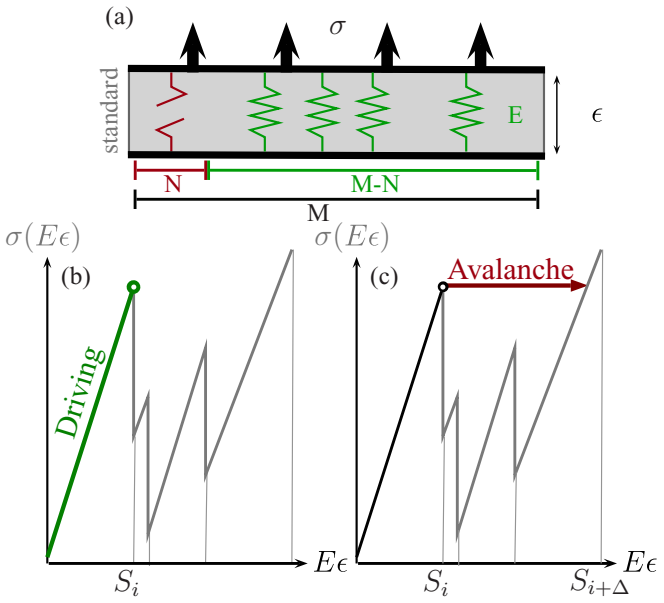

FIG. 1. (a) Schematic representation of the standard DFBM constituted by an ensemble of M parallel elastic-brittle elements, N of which are broken because their $S_i < E\varepsilon$; (b),(c) Sketch of the strain release $E\varepsilon$ due to the breaking of a fiber S_i under quasistatic stress driving, generating an avalanche of size Δ. (c) The avalanche stops when the system regains stability, as represented by the constitutive curve (gray line).

II. FIBER BUNDLE MODELS

A. Standard democratic fiber bundle model (DFBM)

The democratic fiber bundle model (DFBM) is arguably the simplest model able to reproduce avalanche statistics in irreversible fracture mechanics [20,61,76]. As represented in Fig. 1(a), fiber bundle models simulate the mechanical response $[\varepsilon(t)]$ to a tensile stress $[\sigma(t)]$ of a bundle of M initial fibers (l) sharing an externally controlled load. Each fiber is modeled as a coarse grained elastic element with an equal Young's modulus (E) and an independent random limit tolerance to deformation, or strength, S_i usually sampled from an extreme value Weibull distribution with cumulative distribution: $F(S_i < s) = \int_{-\infty}^{s} p(s')ds' = 1 - \exp(-s^m)$, where $p(s')$ is the probability density function. Hence, locally, $E\varepsilon(t) = \sigma_l(t) = M x_l(t) \times \sigma(t)$, where $x_l(t)$ is the fraction of the external stress sustained by the element l, and $\sum_l x_l(t) = 1$. Each fiber will break when $E\varepsilon_i(t) \geqslant S_i$, setting its contribution to the load $x_i(t) \to 0$ and effectively increasing the average $x_l(t)$ for the rest of the ensemble. The nonlinear response of the bundle emerges from the coupling between the values of x_l due to the brittleness S_i of the individual fibers. A good general review on fibrous models can be found in Ref. [77]. The democratic fiber bundle model (DFBM) corresponds to the mean-field solution where all intact fibers contribute equally to the load. The contribution of each fiber can be expressed as a function of the number $N(t)$ of failed fibers over time such that $x_l(t) = \frac{1}{M-N(t)}$ for all l. Since all fibers have the same local load, the number of failed fibers at a given strain value will be given by the number of fibers with strength $S_i < \sigma_l(t)$ and thus $E\varepsilon(t) = \frac{M}{M-N[S_i<E\varepsilon(t)]}\sigma(t)$. Using the numerical cumulative

distribution $F(S_i < E\varepsilon)$, the constitutive equation describing the mechanically stable solutions of the DFBM reads

$$\sigma(E\varepsilon) = [1 - F(S_i < E\varepsilon)]E\varepsilon. \quad (2)$$

Mechanical avalanches will occur as consequence of the metastable solutions in Eq. (2) introduced by the profile of $F(S_i < E\varepsilon)$ under certain driving conditions. Since $F(S_i < E\varepsilon)$ is modified at the breaking of one or several fibers, the mechanical avalanche is caused by the brittle failure of the individual fibers. From now on, we will consider avalanches as the collective instantaneous failure of Δ fibers, Δ being defined as the size of the avalanche.

As a particular case, a macroscopic brittle event will always occur above a stability limit (ε_f,σ_f), that we associate with the macroscopic failure point. In the thermodynamic limit, the failure strain value ε_f under stress driving is given by $E\varepsilon_f := \frac{1-F(E\varepsilon_f)}{p(E\varepsilon_f)}$, where now $F(E\varepsilon_f)$ is a continuous function defined by the sampling strength distribution. In addition, at the microscopic level, $F(S_i < E\varepsilon)$ is a stochastic steplike function and will introduce a stepwise drop in Eq. (2) at the strength S_i of each fiber [see gray lines in Figs. 1(b) and 1(c)], giving rise to an avalanche of size Δ. The probability of size Δ for the DFBM can be obtained as a particular case of the procedure exposed in detail in Sec. III.

Although fiber bundle models were originally designed to simulate the response of fibrous composite materials to tensile stress, successful adaptations towards continuous damage models reported a good agreement with the behavior of shear processes involving plasticity [78], stick-slip dynamics [79], and even granular materials under compression [5]. Thus, one can consider the DFBM as a reliable prototypical and solvable mean-field model of brittle failure [77], able to explain yielding and critical scaling to failure [20,61]. Under stress driving, the statistics of the DFBM are compatible with Eq. (1) as will be discussed in Sec. III in more detail.

B. Temporal correlations and triggering in micromechanical models

As in most conceptual and numerical failure models, the interactions between elements in the DFBM propagate much faster than the variations of the external conditions—corresponding to the quasistatic driving limit—and any other temporal scale of the system. Thus, the transition between stable solutions is driven exclusively by the avalanche dynamics. Since the strength values S_i are independent, the avalanches, defined from the instabilities of Eq. (2), are uncorrelated. The temporal clustering observed in nature and experiments can be reproduced in conceptual models by the introduction of a temporal scale interfering with the avalanche propagation. For example, correlations have been observed in stick-slip models with dissipation [76,80], yet they were shown not to be a consequence of event-event triggering but a consequence of slow temporal variations in the Poisson intensity or synchronization [81]. Power-law waiting times can also be artificially constructed by a nonquasistatic driving and a thresholding of the activity [82–84], without requiring the involvement of any triggering or aftershock process.

Event-event triggering or aftershock sequences and the associated temporal correlations are commonly reproduced by introducing additional temporal scales affecting the propagation of the avalanches, without requiring to break the quasistatic condition. In the case of fracture and stick-slip processes, it has been proposed that temporal scales are introduced by the nonlinear rheological or tribological behaviors of the coarse-grained elements of the material [55,56]. As examples, micromechanical models reproduce aftershock sequences by incorporating rate and state-dependent friction [63], damage rheology [64], viscoelasticity [9,65,67,70], or a viscous drag [66]. In general terms, a partial delay in the response of the material such as velocity hardening or viscoelastic creep will introduce an effective transient hardening of the thresholds [55,64,68,69,85] splitting the otherwise instant transition in a cascade of smaller temporally correlated avalanches [55]. The relaxation of this hardening towards the equilibrium state can give rise to the temporal correlations between avalanches [86] mimicking those observed in aftershock sequences. Thus, this process can capture the temporal features associated with event-event triggering observed in seismic catalogs [59,71,72,87] and AE experiments [26,34–37,88,89]. On the other hand, this transient hardening corresponds to a dissipation mechanism coupled to the dynamics, thus, affecting criticality. Hence, both the presence of correlations and the lack of criticality at failure might be reproduced by the introduction of transient hardening in micromechanical models that would normally reproduce critical failure.

C. Formulation of the generalized viscoelastic DFBM

Here, we derive the mean-field solutions to a transient hardening model [68] by explicitly incorporating generalized viscoelasticity into the DFBM. We compare the analytical solutions with the standard DFBM—i.e., without viscoelasticity—to understand how this mechanism of transient hardening affects the statistical properties of avalanches. Specifically, we discuss its ability to explain (i) the presence of ASR without a divergence of scales at failure—i.e., critical failure—and (ii) temporal correlations between events.

An interesting aspect of this model is the substitution of the elastic fibers with generalized Zener solid elements [90], as schematically shown in Fig. 3(a). These elements are equivalent to a fractal viscoelastic model [91], stable under stress and strain driving and able to describe realistic memory relaxation processes, as observed, for example, in amorphous solids [92,93]. This viscoelastic model introduces a physically based mechanism of transient hardening (as will be discussed in Sec. II F) in the microscopic elements with brittle failure.

Each of the elastic brittle elements of the standard DFBM ($\sigma_e = E\varepsilon$) is now coupled in parallel to a generalized Maxwell element [94] (see left panel of Fig. 2). The generalized Maxwell element consists of a secondary elastic spring ($\sigma_m = E_m\varepsilon$) coupled in series to a Scott-Blair springpot [95,96], instead of the usual viscous dashpot. While the mechanical response of the standard dashpot reads $\sigma_X = \eta d\varepsilon_X/dt$, where η is the viscosity, the generalized element involves fractional derivatives ($\sigma_X = X d^\alpha \varepsilon_X/dt^\alpha$) with physical fractional dimensions $0 \leqslant \alpha \leqslant 1$ and a general complex modulus X instead of η. The constitutive relations of each generalized Zener solid element can be obtained from the mechanical equilibrium between the individual parts as represented in Fig. 2. The conditions

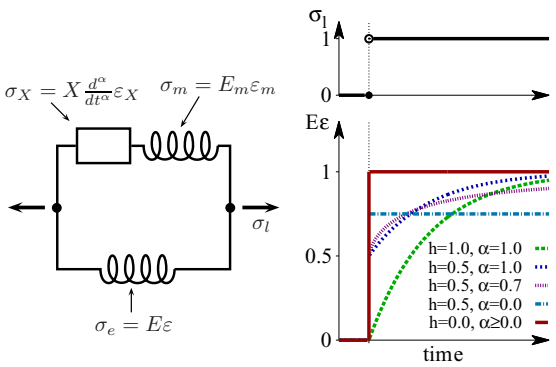

FIG. 2. Left: schematic representation of the generalized Zener element. Right: Temporal response $E\varepsilon$ of the generalized Zener element to a stepwise increase in the load σ_l. Five example behaviors are represented for different values of $0 \leqslant h \leqslant 1$ and $0 \leqslant \alpha \leqslant 1$ (see main text for details).

$\sigma_m \equiv \sigma_X$, $\varepsilon \equiv \varepsilon_m + \varepsilon_X$, and $\sigma_l \equiv \sigma_e + \sigma_m$ have to be satisfied, leading to the constitutive equation

$$\left[1 + \frac{X}{E_m}\frac{d^\alpha}{dt^\alpha}\right]\sigma_l = \left[1 + \frac{X(E_m+E)}{E_m E}\frac{d^\alpha}{dt^\alpha}\right]E\varepsilon. \quad (3)$$

By defining $\tau^\alpha := X(E_m+E)/(E_m E)$, the strain response to a sudden increase in stress $\Delta\sigma$ at time 0—i.e., creep response—$\Delta\varepsilon(t) = J_{\rm GZ}(t)\Delta\sigma_l$ has the explicit solution [97]:

$$J_{\rm GZ}(t) = \frac{1}{E}\left[\frac{E}{E_m+E} + \frac{E_m}{E_m+E}\{1 - \mathbf{E}_\alpha[-(t/\tau)^\alpha]\}\right]$$
$$= \frac{1}{E}\left[1 - \frac{E_m}{E_m+E}\mathbf{E}_\alpha[-(t/\tau)^\alpha]\right], \quad (4)$$

where $\mathbf{E}_\alpha(z) := \mathbf{E}_{\alpha,1}(z) = \sum_{n=0}^{\infty}\frac{z^n}{\Gamma(\alpha n+1)}$ denotes the so-called Mittag-Leffler function. Viscoelasticity adds a correction term to the elastic response $J_{\rm E} = 1/E$. This correction decreases as a stretched exponential for short times, since $\lim_{t/\tau\to 0^+}\mathbf{E}_\alpha[-(t/\tau)^\alpha] = e^{-(t/\tau)^\alpha/\Gamma(\alpha+1)}$ and evolves towards a power-law decay with exponent α for $0 < \alpha < 1$, since $\lim_{t/\tau\to+\infty}\mathbf{E}_\alpha[-(t/\tau)^\alpha] = (t/\tau)^{-\alpha}/\Gamma(1-\alpha)$. By simplifying the transient term $\mathbf{H}_\alpha(t/\tau) := \frac{E_m}{E_m+E}\mathbf{E}_\alpha[-(t/\tau)^\alpha]$, the response of each fiber to a sudden increase in the local stress $\Delta\sigma_l$ reads

$$E\Delta\varepsilon(t) = [1 - \mathbf{H}_\alpha(t/\tau)]\Delta\sigma_l. \quad (5)$$

Here, the transient term evolves from a positive value:

$$h := \mathbf{H}_\alpha(0) = \frac{E_m}{E_m+E} \quad (6)$$

to $\mathbf{H}_\alpha(t/\tau \gg 1) \to 0$. A sudden increase in the local stress will induce an initial sudden increase in strain of the elastic element $E\Delta\varepsilon(0^+) = \frac{E}{E+E_m}\Delta\sigma_l$ which is lower than in the standard DFBM $[E\Delta\varepsilon(0^+) = \Delta\sigma_l]$. The rest of the elastic energy is retained by the springpot element and slowly released to the spring element during the creeping phase. This creep response shares similarities with the addition of viscoelasticity to the elastic rebound model proposed in Ref. [85]. The creeping time of the springpot introduces a third temporal scale to the model, apart from the interaction between fibers and the driving. This additional temporal scale is responsible for the emergence of temporal correlations in this model (Sec. IV D). We consider that the interactions between fibers are much faster than the relaxation of the springpot. Under quasistatic driving, all temporal scales are much faster than the driving. This implies that the response value for the standard DFBM is reached before the system is driven again, since $\mathbf{H}_\alpha(t/\tau \gg 1) \to 0$.

D. Parameters of the generalized viscoelastic DFBM

As represented, the Zener solid element has three free parameters: τ, α, and h. Within the framework of our model, the generalized relaxation timescale τ is arbitrary as we assume a timescale separation between the quasistatic driving, the relaxation time, and the instantaneous avalanche propagation.

The role of the parameters h and α is represented in the right-hand panel of Fig. 2. The fractional dimension α controls the profile of the relaxation process. By imposing $\alpha = 1$ we recover the standard Zener element, where $X := \eta$ representing a viscous dashpot and the corresponding term $\mathbf{H}_1(t/\tau) = h\exp(-t/\tau)$. Lower values of α imply a more complex memory in the relaxation that cannot be simplified in an exponential decay. Instead, the memory is characterized by a power-law decay. For $\alpha \to 0^+$ the quasistatic condition starts to fail: viscoelasticity affects the propagation of the avalanche and relaxes at times long enough to interfere with the driving. In the extreme case of $\alpha = 0$ this transient term becomes permanent and $\mathbf{H}_0(t/\tau) = h/2$. Note that this case is singular since $\mathbf{H}_{\alpha>0}(0) = h$ for any other value of α.

Overall, α controls the temporal correlations between avalanches but, excluding the case $\alpha \approx 0$, it only has a minor role on their size and number. Instead, these are controlled by the hardening parameter h. For $h = 0$, equivalent to setting $E_m \ll E$, we recover the elastic response. We use this case as a benchmark to the standard DFBM in our numerical simulations. For $E \ll E_m$ [68], we recover a generalized Kelvin-Voigt element, with $h = 1$. This case imposes continuity in ε and hence all fibers break individually, since a sudden increase in σ_l does not generate a sudden stress drop. The implementation of fiber bundle models with Kelvin-Voigt elements is briefly discussed in Ref. [77]. Here, we solve analytically the more general viscoelastic DFBM (GVE-DFBM) by using the mechanical behavior of the individual generalized Zener elements in the constitutive equation of the DFBM [see Fig. 3(a)].

E. Constitutive equation of the GVE-DFBM

Considering the stress variations due to fracture in Eq. (5) and equal load sharing $[\sigma_l = \sigma/(1-F)]$, the constitutive equation of the GVE-DFBM will match Eq. (2) when all terms $\mathbf{H}_\alpha(t/\tau) \to 0$, i.e., on the timescale of the quasistatic driving. Directly after the breaking of fibers, the constitutive equation depends on the historical sequence of the recent avalanches $\{j\}$ occurring at the frozen value of σ, and can be expressed as

$$E\varepsilon(t) = \sigma(t)\left(\frac{1}{[1-F(E\varepsilon)]} - \sum_{S_j<E\varepsilon}\phi_j(t-t_j)\right), \quad (7)$$

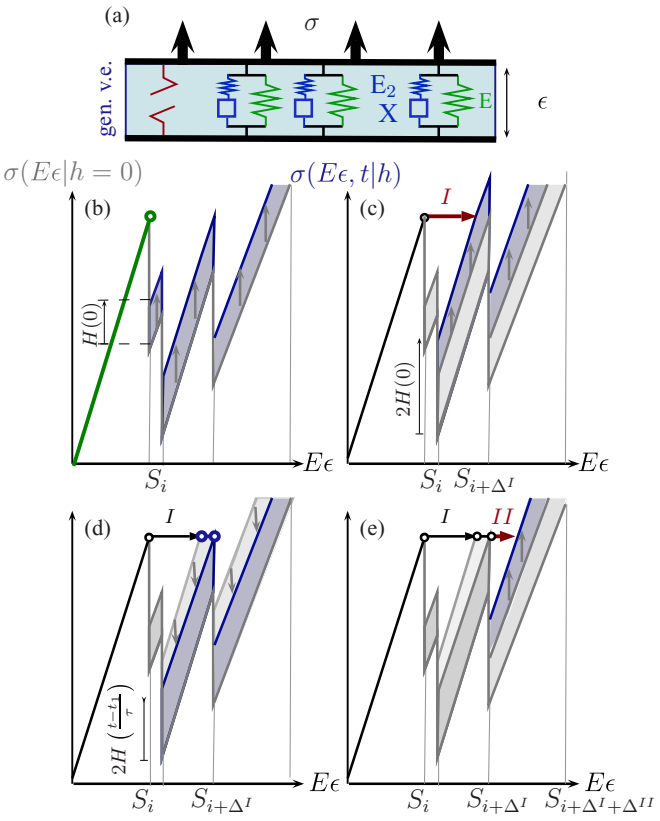

FIG. 3. (a) Schematic representation of the generalized rheological democratic fiber bundle model (GVE-DFBM), where the elastic element has been substituted by a generalized Zener solid element. (b)–(e) Sketch of an avalanche process in the GVE-DFBM with the same fibers considered in Fig. 1. (b) The system is hardened a factor $H(0)$ for each failed fiber (blue lines). (c) The initial avalanche, of size Δ^I, stops sooner than in the standard DFBM. (d) During the creeping phase and without driving, the hardening is relaxed just enough to activate the next failure. (e) The process is repeated until all the Δ fibers of Fig. 1 are broken. All transient terms are relaxed to 0 before resuming the quasistatic driving. While part of the brittle deformation in the standard DFBM model occur as creep in the GVE-DFBM, the number of broken fibers remains the same.

where the terms

$$\phi_j(t-t_j) := \frac{\delta F_j \mathbf{H}_\alpha\left(\frac{t-t_j}{\tau}\right)}{[1-F(S^-_{j+\Delta_j})][1-F(S^-_j)]} \tag{8}$$

contain the contribution of each preceding avalanche j, with integer size $\Delta_j := M\delta F_j$ initiated at strength values S^-_j. Notice that Eq. (7) is still valid even if the quasistatic condition is not met. However, under fast driving, the terms $\phi_j(t-t_j)$ cannot be neglected and Eq. (7) only coincides with Eq. (2) at the very beginning of the external driving, i.e., when no events have occurred yet.

Contrary to Eq. (2), the constitutive equation (7) has a temporal dependence on the history of the process in all cases and cannot be simplified as a function of state. Thus, the avalanche activity rate will exhibit temporal correlations, absent in the standard DFBM.

F. Viscoelasticity as a transient hardening

While the formulation of the GVE-DFBM involves a very specific physical process, the effect of viscoelasticity with respect to the standard DFBM can be generalized to the conceptual idea of "transient hardening" [55,68], as we prove in this section. In the standard DFBM, the instantaneous failure of a system fraction δF at $S = E\varepsilon$ introduces a drop in the constitutive Eq. (2) corresponding to

$$\delta\sigma_{\rm std} = -E\varepsilon\delta F. \tag{9}$$

In the GVE-DFBM [Eq. (7)] the same event will cause a stress change:

$$\delta\sigma = \frac{\delta\sigma_{\rm std}[1-\mathbf{H}_\alpha(t/\tau)]}{\left[1-(1-F)\sum\phi\right]\left[1-(1-F-\delta F)\left(\sum\phi+\phi_s\right)\right]}, \tag{10}$$

where $\phi_s = \frac{\delta F h}{[1-F(S^-_{j+\Delta})][1-F(S^-_j)]}$ is the ϕ term due to the latest failure of δF. We have relabeled the term $F := F(E\varepsilon^-)$. In the thermodynamic limit, $\delta F/(1-F) \ll 1$, and the denominator can be approximated as 1 at the lowest order. Thus, in this limit the mechanical response [Eq. (10)] reduces to

$$\delta\sigma \approx \delta\sigma_{\rm std}[1-\mathbf{H}_\alpha(t/\tau)]. \tag{11}$$

Since the stress drop is reduced with respect to $\delta\sigma_{\rm std}$, the system regains stability with a lower deformation than the standard DFBM [see Figs. 3(c)–3(e)], instantly hardening the bundle by an amount $\mathbf{H}_\alpha(0)$. Hence, we can interpret the transient term $\mathbf{H}_\alpha(t/\tau)$ in Eq. (5) as a transient hardening with respect to the standard DFBM, increasing temporally the effective strength in σ of all the surviving elements.

G. Origin of aftershocks

The history dependence in the constitutive equation is a mechanism able to generate temporal correlations, that can be expressed in terms of a triggering point process, where each avalanche is either a "background" event activated by the external driving or a "triggered" event when it is a direct consequence of previous activity. This is consistent with the event-event triggering or aftershock picture typically invoked for seismic events [71,72,87] and AE events [34,37,74] to explain temporal correlations. Specifically, the rate of events triggered by a given event decays over time, with a typical power-law profile that is consistent with the relaxation of generalized viscoelasticity [98]. Figures 3(c)–3(e) represent schematically the avalanche process in the GVE-DFBM (blue curve) in comparison to the standard DFBM (gray curve). The breaking of the fibers at $S_{i+\Delta^I}$ in Fig. 3(d), retarded by effect of hardening, occurs at the same stress σ that triggered the primary avalanche [at S_i in Fig. 3(b)], since we consider that the relaxation time needed to activate the secondary avalanche is much faster than the quasistatic driving. Thus, the driving is not directly responsible for the secondary avalanche in $S_{i+\Delta^I}$. Instead, it is the failing of the elements broken in the avalanche at S_i (this one due to the driving) which triggers the failure. Thus, we can classify the events into background (event I starting at S_i in this example) and triggered (event II starting at $S_{i+\Delta^I}$ in this example).

While the temporal evolution has changed on the timescale of the relaxation, the $\sigma(\varepsilon)$ diagram is invariant to transient hardening. As a consequence, considering the same driving conditions, a given avalanche in the standard DFBM is split into a cluster of causally correlated avalanches in the GVE-DFBM. When all the fibers forming the avalanche in the standard DFBM—now, the cluster—have been broken, all terms $\phi_j(t)$ are relaxed to zero. This imposes temporal independence between clusters, since Eq. (7) is equivalent to Eq. (2) in that case.

Since the interactions are mean field, all correlations between avalanches are determined by a scalar relation between the activation strengths. Independently of the value of h, an individual fiber with strength S_j will break as a consequence of a previously broken fiber S_k if $S_j[1 - F(S_k) - 1/M] < \sigma < S_j[1 - F(S_k)]$. Depending on the value of h, the breaking of S_j will occur either within the same avalanche or within a latter triggered avalanche (i.e., aftershock) within the same cluster, only when $h > 0$. Since this stability condition is derived from the distribution of S_i, this separation between triggered and background events still holds when σ has evolved between avalanches, i.e., outside the quasistatic limit. Hence, mean-field models are unable to generate the superposition of complex triggering trees identified in natural phenomena [72,73,99,100] and modeled in spatiotemporal stochastic point processes [71,87,101]. Instead, all aftershocks triggered due to the breaking of a given fiber S_k are correlative in time and occur in the same cluster.

However, even the MF approximation is able to render the power-law temporal statistics (see Sec. IV D), supporting the link between triggering process and the phenomenological observations of aftershocks in AE experiments and seismicity. From the analytical results derived in the following sections, we can argue that the details regarding the structure of the triggering trees shall not have a significant impact on the shape of the avalanche size distribution in the thermodynamic limit.

III. MEAN-FIELD UNIVERSALITY CLASS FOR FRACTURE WITH TRANSIENT HARDENING

As mentioned in Sec. II G, the stress value for an avalanche to occur in the standard DFBM coincides with the stress value of a cluster in the GVE-DFBM. The constitutive curves of both models are indistinguishable in the thermodynamic limit, and so is the coarse grained effective inverse modulus $G^{-1} = d\varepsilon/d\sigma$ as well as the moment released per time unit $d\Delta/dt$. However, the number of avalanches and their statistical properties have been strongly altered. Avalanches tend to be smaller [Eq. (10)] due to the effect of hardening and yet, as we will prove now, all avalanche statistics fall inside the same universality class, regardless of the value of h.

A. Interpretation of avalanche sizes as hitting times in a stochastic process

Under general driving conditions, an avalanche starting at the failure of fiber i with strength S_i will stop at the first fiber $i + \Delta_i$ with strength $S_i + \delta s$ such that $\sigma(S_{i+\Delta_i}) > \sigma(S_i) + \delta\sigma(t_{i+\Delta_i} - t_i)$, where $\delta\sigma(t_{i+\Delta_i} - t_i)$ is the increase in stress between the breaking of fibers i and $i + \Delta$ that will depend on the external driving condition. Since we are considering quasistatic stress driving, the propagation of the avalanche is much faster than any variation of the stress and the term $\delta\sigma(t_{i+\Delta_i} - t_i) \equiv 0$. Thus, the size of the avalanche Δ_i is defined as the number of broken fibers from a process of record dynamics and related to the difference in the fraction of broken fibers ($\delta F := F_{i+\Delta} - F_i$) as $\delta F \equiv \Delta/M$. Since the propagation of the avalanche is much faster than the viscoelastic relaxation, the contribution to the transient term of all the fibers broken within the same avalanche is $\phi_i = \frac{\delta F \mathbf{H}_\alpha(0)}{(1-F_i)(1-F_i+\delta F)}$. From the constitutive equation (7), the avalanche stops when

$$\frac{\delta s}{\delta F} > \frac{1}{\left[1 - (1 - F_i)\sum_j \phi_j(t - t_j)\right]} \times \frac{S_i[1 - \mathbf{H}_\alpha(0)]}{(1 - F_i - \delta F)}. \tag{12}$$

The right-hand side of the equation is constituted by two terms. The term $\frac{1}{[1-(1-F_i)\sum_j \phi_j(t-t_j)]}$ contains the effect of previous avalanches on the size of the current one and is static during the propagation of the avalanche thanks to the separation between temporal scales. The other term on the right-hand side of Eq. (12) includes a dependence on the size of the current avalanche (δF) because the macroscopic state of the system is modified during the propagation of the avalanche. This variation will have a significant effect when the size of the avalanche is comparable to the system size, but not if the avalanche is small. Let us consider, for now, that all avalanches are small compared to the system size. For the propagating avalanche, $1 - F_i - \delta F \sim 1 - F_i$ and for all previous avalanches $(1 - F_i)\sum_j \phi_j(t - t_j) \ll 1$. The whole right-hand side of Eq. (12) can then be expressed as a single quantity b. This quantity is a function of the state of the system at S_i and constant during the propagation of the avalanche:

$$b(S_i|h) := \frac{S_i}{1 - F_i}(1 - h). \tag{13}$$

The left-hand side of Eq. (12) can be redefined in a dimensionless form. By definition, $\delta F := \Delta/M$. Since the values of S_i are independent and identically distributed, the increment δs between Δ consecutive strengths is a Poisson process of Δ trials at rate $Mp(s)$. The dimensionless form of Eq. (12) for this general representation of the transient hardening model reads

$$\frac{\xi(\Delta_i)}{\Delta_i} > B(S_i|h), \tag{14}$$

as represented in Fig. 4(a), where $B(S_i|h) := p(S_i)b(S_i|h)$ and $\xi := Mp(s)\delta s$ is a Poisson process of rate 1. Given a single realization of strengths at fixed h, once an avalanche has started at S_i, the value $B(S_i)$ acts as a constant threshold and the distribution of avalanches in the GVE-DFBM is equivalent to the distribution of first hitting times of a random Poisson counting process $\xi(\Delta)$ to the moving boundary $B(S_i)\Delta$.

For $B > 1$ there is a macroscopic probability that an avalanche grows to an infinite size. We associate this supercritical regime to a brittle failure event. For $B < 1$ the probability of an infinite avalanche is 0, and the distribution

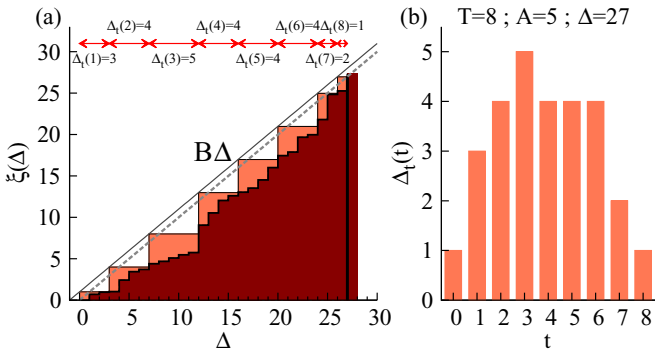

FIG. 4. (a) Example of an avalanche defined as the hitting times of a stationary random counting process $\xi(\Delta)$ to the boundary $B\Delta$. Maroon area shows the landscape $\xi(\Delta)$ drawn from random Poisson increments at each elementary step Δ. The avalanche stops at the first Δ value with $\xi(\Delta) > B\Delta$ represented as a dashed gray line. The salmon area represents the elements failing at the time unit, with values $\xi(\Delta) < B[\Delta(t-1)+1]$ (black solid line). (b) The temporal profile of the same avalanche, defining the amplitude A, duration T, and size Δ (see Sec. III B).

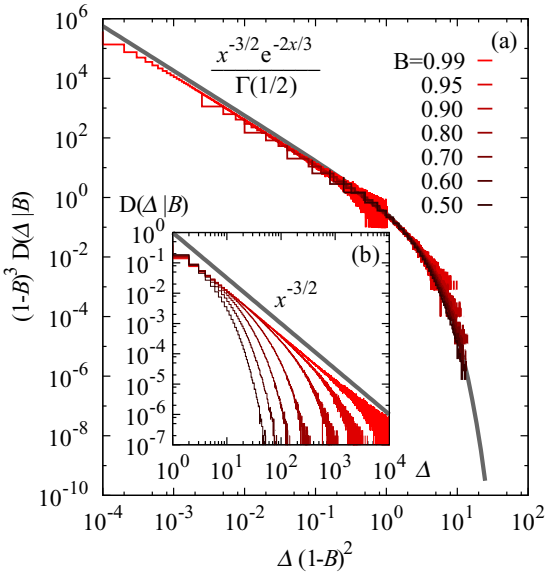

FIG. 5. Distribution of $N = 10^7$ hitting times for the Poisson process ξ_Δ to the boundary $B\Delta$ tapped at $\Delta = 10^4$ for different values of B. (a) Scaling according to Eq. (16) compared to the ansatz (grey thick line) in Eq. (17). (b) Distribution before scaling, compared to the power law expected by $B = 1$ (gray thick line).

of finite avalanche sizes can be approximated as a generalized homogeneous function:

$$D(\Delta; B)d\Delta = \Delta^{-\kappa_\Delta}\,\mathcal{D}(\Delta|1-B|^{\beta_B})\,d\Delta \tag{15}$$

$$= |1-B|^{\kappa_\Delta\beta_B}\,\widetilde{\mathcal{D}}(\Delta|1-B|^{\beta_B})\,d\Delta, \tag{16}$$

where κ_Δ and β_B are universal exponents, and $\widetilde{\mathcal{D}}(\Delta|1-B|^{\beta_B}) := (\Delta|1-B|^{-\beta_B})^{\kappa_\Delta}\mathcal{D}(\Delta|1-B|^{\beta_B})$ and $\mathcal{D}(\Delta|1-B|^{\beta_B})$ are scaling functions. This scaling term diverges exactly at $B_c = 1$, which defines a critical point with scale-free avalanches. It is important to remember that B is constant only in the regime of small avalanches. In both the standard DFBM and GVE-DFBM, this limit can be achieved asymptotically close to a critical point—where avalanches are scale free—by increasing the size of the system. In the thermodynamic limit ($M \to \infty$), the yielding process up to the critical point is well defined by Eq. (14). But, according to Eq. (12), at criticality and above, when $B(\delta F \to 0) \geqslant 1$, the avalanche might grow to sizes such that $B(\delta F) > B(\delta F \to 0)$ and, thus, the system is, by definition, supercritical. Although $B = 1$ is critical, the critical point in the DFBM is not well defined because of the coupling between the avalanche size (Δ) and the state of the system (B). From now on, the reader shall keep in mind that the expression (14) and the following derivations are valid for $B < 1$ in the DFBM.

Figure 5(b) shows the numerical distribution of return times (Δ) for different values of B. The probability distribution functions collapse onto a single universal function given the scaling relations with B stated in Eq. (16), as shown in Fig. 5(a). The fitted critical exponents are $\kappa_\Delta = 3/2$ and $\beta_B = 2$. The exponent $\kappa_\Delta = 3/2$ is ubiquitous in the distribution of avalanche sizes in mean-field models. The exponent β is usually defined as a function of the driving mechanism and the relation with B has to be derived, as shown in the next section for the case of the DFBM.

Since Eq. (14) is dimensionless, all the information, including the distribution of avalanches, is fully determined by the scalar term $f_B := 1 - B$ measuring the distance a critical point. In the case of the transient hardening model, the value of B is defined in the thermodynamic limit given a hardening h, a strain value s/E, and the sampling distribution of S_i. Since the functional form of $\mathcal{D}$ is invariant to the explicit dependence of B with the state of the system, any model that can be represented as Eq. (14) fulfills the scaling relation (16). Considering the distribution represented in Fig. 5(a) the specific functional form of $\mathcal{D}$ can be approximated to the ansatz:

$$\mathcal{D}(x) = \exp(-3x/2)/\,\Gamma(-0.5). \tag{17}$$

However, one can show that this approximation is inadequate to measure some quantities such as $\langle\Delta\rangle$, especially for $B \ll 1$, due to the discrete nature of Δ. Instead, we use the following ansatz for the dependence of the statistical moments on f_B:

$$\langle\Delta^n|f_B\rangle = f_B^{(\kappa_\Delta-1-n)\beta_B}. \tag{18}$$

Therefore, Eq. (18) will replace Eq. (17) when possible to compare analytical and numerical results. As a consequence of this power-law relation, even if the explicit dependence of a model on B is unknown, Eq. (16) can be rewritten in terms of the first statistical moment $\langle\Delta|f_B\rangle = f_B^{(\kappa_\Delta-2)\beta_B}$ as

$$D(\Delta;\langle\Delta\rangle)d\Delta = \langle\Delta\rangle^{\frac{\kappa_\Delta}{\kappa_\Delta-2}}\widetilde{\mathcal{D}}(\langle\Delta\rangle^{\frac{1}{\kappa_\Delta-2}}\Delta)d\Delta \tag{19}$$

for a fixed f_B. This expression depends only on the specific exponent κ_Δ with MF values $\frac{\kappa_\Delta}{\kappa_\Delta-2} = -3$ and $\frac{1}{\kappa_\Delta-2} = -2$. Notice that this expression is more general than Eq. (16) and may be also fulfilled by other models incompatible with Eq. (14).

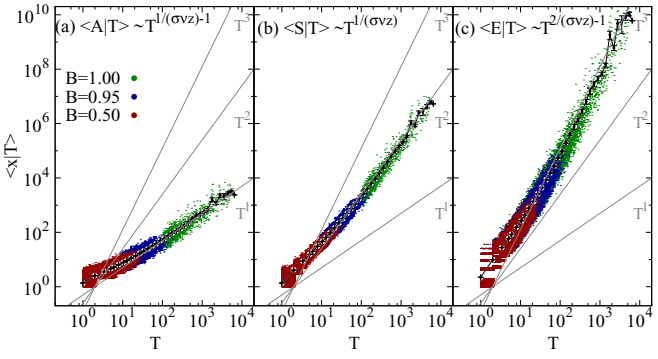

FIG. 6. Scatter plots of magnitude pairs: (a) A,T, (b) S,T, (c) E,T found for different values of B. (Since the values are discrete a uniform unitarian jitter in the x and y axes has been added to better visualize the density of the point clouds.) The conditional averages $\langle x|T\rangle$ are shown for $B = 1$ (black error lines). The expected relations derived from Eq. (20) are consistent with an exponent value $\sigma\nu z = 1/2$.

B. Mean-field exponents

In order to fully characterize the universality class (UC), we define a time unit within the temporal scales of avalanche propagation and associate a temporal profile to the avalanche propagation by designating the causality treelike structure between the failing fibers. In terms of a DFBM, the breaking of an original fiber at time unit 0 can cause the breaking of a number of fibers during time unit 1. Such fibers will cause the breaking of other fibers at time unit 2, etc. The temporal profile at time t is determined by the number Δ_t^i of fibers with associated values $\xi[\Delta(t-1)+\Delta_t^i] < B[\Delta(t-1)+1]$, i.e., all the values of ξ that can be activated by the state of the system at time $t-1$. In Fig. 4(a), the salmon areas illustrate the set of fibers breaking together in a time unit (until $\xi[\Delta(t-1)+\Delta_t^i]$ hits the value $B[\Delta(t-1)+1]$) given by the black solid line). The intensity of the temporal profile is represented with arrows in Fig. 4(a), and histograms in Fig. 4(b). Apart from the avalanche size $\Delta^i = \sum_{t=0}^{T} \Delta_t^i(t)$, the temporal profile $\Delta_t^i(t)$ allows us to define additional variables: a duration T^i, as the number of time units; an amplitude A^i corresponding to $\max[\Delta_t^i(t)]$; and also an energy $E^i = \sum_{t=0}^{T} [\Delta_t^i(t)]^2$, usually related to the seismic release and acoustic emission measurements in the literature [102].

Assuming that the process defining the hitting times is scale invariant over a broad range of scales, the average avalanche profile must scale with the duration such that

$$\langle \Delta_t(t)|T\rangle = T^{1/\sigma\nu z-1}\Phi(t/T). \tag{20}$$

The average relation between the four magnitudes can be summarized as

$$\langle A|T\rangle \sim T^{1/\sigma\nu z-1} \quad \langle \Delta|T\rangle \sim T^{1/\sigma\nu z} \quad \langle E|T\rangle \sim T^{2/\sigma\nu z-1}. \tag{21}$$

The numerical results of the conditional averages are shown in Fig. 6. Although the density distributions depend on B, the average relationships between magnitudes is conserved and agrees with Eq. (20) given a value $\sigma\nu z = 1/2$, coinciding with the mean value for stick-slip models [49].

IV. SIMULATION RESULTS

A. Interpretation of B in terms of the driving in the standard and GVE-DFBM

In each specific model of critical failure, the particular exponent β associated to the distance to failure is determined by the explicit relation between B and the mechanism of external driving such as a constant stress (σ) or strain (ε) rate driving. In such cases, we can formulate the time to failure in terms of distance to the macroscopic failure point in strain: $E\varepsilon_f = \frac{1-F(E\varepsilon_f)}{p(E\varepsilon_f)}$, or stress: $\sigma_f = \frac{(1-F(E\varepsilon_f))^2}{p(E\varepsilon_f)}$. In the case of the GVE-DFBM, the general relation of B with strain can be obtained to a good approximation in the thermodynamic limit by expanding B around the failure point:

$$B = (1-h)\left[1 - f_\varepsilon\left(2 + \varepsilon_f \frac{d}{d\varepsilon}\ln[p(E\varepsilon)]\Big|_{\varepsilon_f}\right) + O(f_\varepsilon^2)\right], \tag{22}$$

where $p(E\varepsilon)$ is the strength (S_i) distribution evaluated at $E\varepsilon$. This relation is linear in a first order approximation. The strength sampling distribution only affects the constant term $2 + \varepsilon_c \frac{d}{d\varepsilon}\ln[p(E\varepsilon)]|_{\varepsilon_c} =: 2A$. As specific cases, if S_i is uniformly distributed, $A = 1$, while for a Weibull distribution, $A = 1 + m/2$. Considering the first order approximation (22), $f_B \approx 2(1-h) f_\varepsilon A + h$ and, at the yield point (when $f_\varepsilon^f = 0$), $f_B^f \approx h$. Critical failure only occurs for $h = 0$, corresponding to the standard DFBM. The model with $h = 0$ is critical in terms of Eq. (1) with the exponent $\beta_\varepsilon = 2$. As a particular result, we notice that the characteristic scale at failure ($f_\varepsilon = f_\sigma = 0$) scales with h as $\langle \Delta|h\rangle \sim h^{-1}$. Instead, the MF solution of stick-slip models reports a scaling $\langle \Delta|\epsilon\rangle \sim |\epsilon|^{-2}$ [55], with h being equivalent to $-\epsilon$. The discrepancy in this exponent is discussed in the next section.

We can find the relation with stress (σ) by expanding the constitutive equation around ε close to the critical point. Under quasistatic driving, $\sigma(E\varepsilon)$ is equivalent to Eq. (2) and around ε_f reads

$$f_\sigma = f_\varepsilon^2\left(1 + \frac{\varepsilon_f}{2}\frac{d}{d\varepsilon}\ln[p(E\varepsilon_f)]\right) + O\left(f_\varepsilon^3\right). \tag{23}$$

Thus, $f_\sigma \approx A f_\varepsilon^2$ and $f_B \approx (1-h)(A f_\sigma)^{1/2} + h$. For the standard DFBM, we find critical failure [Eq. (1)] with $\beta_\sigma = 1$, as expected from the mean-field solution of the standard DFBM [76]. As an example, for a Weibull distribution and standard ($h = 0$) conditions: $f_B(f_\varepsilon) = 1 - (1 - f_\varepsilon)$ and $f_B(f) = 1 + W(-\frac{(1-f_\sigma)^m}{e})$ where $W(x)$ is the Lambert function, inverse of $x = W\exp(W)$. We can expand f_σ in terms of f_B by inverting this expression:

$$f_\sigma = 1 + (f_B - 1)\exp(f_B) = \frac{f_B^2}{2m} + \frac{f_B^3}{3m} + O\left(f_B^4\right), \tag{24}$$

thus satisfying the approximate relation $f_\sigma \sim f_B^2$, as expected based on the approximations in Eqs. (23) and (22).

B. Distribution of avalanche sizes

Given the distribution of Δ (16) and considering the relation between σ and B derived from Eqs. (23) and (22),

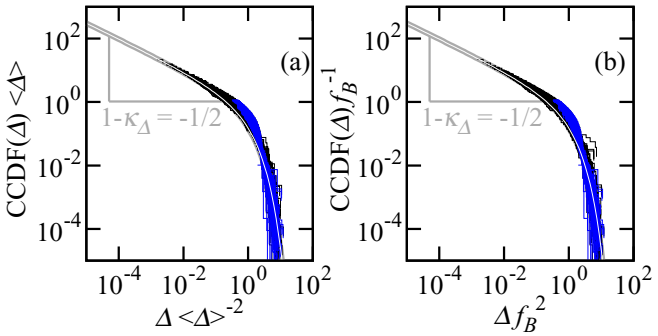

FIG. 7. Complementary cumulative distribution function (CCDF) of avalanche sizes scaled by (a) their mean value ($\langle\Delta\rangle$) and (b) distance to criticality (f_B), obtained by the numerical simulations of the GVE-DFBM with $m = 1$ (standard Zener elements) and $M = 10^7$ evaluated in intervals of σ. We compare the results for $h = 0.4$ (in blue) with the standard DFBM ($h = 0$ in black) and the universal distribution for the analogous hitting time problem according to Eq. (17) (gray thick lines).

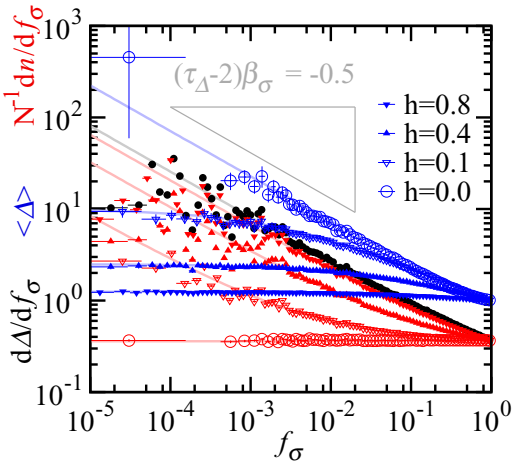

FIG. 8. Normalized activity rate (red) as the number of events for unit of time ($N^{-1}dn/df_\sigma$), average avalanche size ($\langle\Delta\rangle$ in blue), and number of fibers failed for unit of time $d\Delta/dt$ for the GVE-DFBM with values of $h = 0.0$, 0.1, 0.4, and 0.8. Light lines serve as a guide to the eye with the analytical solution found for the thermodynamic limit. The temporal scale is expressed in terms to the distance to failure in stress, in order to empathize the agreement with the power-law divergences at the failure point.

we can forecast the expected distribution of sizes, durations, amplitudes, and energies for the GVE-DFBM model as a function of the distance to the critical point under stress driving, f_σ. As a specific case, the distribution of avalanche sizes, matching the results represented in Fig. 5, for the standard DFBM will depend explicitly on the distance to the failure stress as

$$D(\Delta; f_\sigma)d\Delta = \Delta^{-3/2}\,\mathcal{D}(\Delta f_\sigma)\,d\Delta \tag{25}$$

and, thus, differ from the mean-field solution for stick-slip models, where the characteristic function scales with Δf_σ^2. We have shown that this specific exponent—usually referred to as $1/\sigma$ in the literature—depends on the relation $B(\sigma)$. Unlike fracture models, stick-slip models restitute or "stick" failed elements, giving rise to a characteristic stationary flow regime under strain driving. If one were able to express the MF stick-slip model in terms of Eq. (14), the relation $B(\sigma)$ would differ from Eq. (24) because of that.

Figure 7 shows the scaling in both f_B and $\langle\Delta\rangle$ of the numerical cumulative distribution CCDF(Δ) for $h = 0$ and $h = 0.4$ in a DFBM with a Weibull sampled strengths s_i with $m = 1$ and $\alpha = 1$ (see the Appendix for simulation details). The results fit well the normalized ansatz (17) for the UC (14) as a solution to Eq. (16). As expected, Fig. 7(b) showing the scaling factor with f_B deduced from Eq. (24) is almost indistinguishable from Fig. 7(a) showing the scaling with $\langle\Delta\rangle$. This result confirms that the predictions derived from the UC in Sec. IV A are valid in the case of the GVE-DFBM.

C. Subcritical failure and foreshocks

Thanks to the explicit evolution of f_B in Eq. (16), we can provide an explanation for the observed lack of divergence in the mean avalanche magnitudes—either amplitude, size, or energy—in processes exhibiting accelerated seismic release (ASR) proportional to the yielding in the constitutive equation (7). While the number of broken elements over time [$d\Delta/dt(f) = \sum\langle\Delta\rangle(f)dn/dt(f)$] is independent of the rheology in the quasistatic and thermodynamic limit, the evolution of $dn/dt(f)$ and $\langle\Delta\rangle(f)$ will depend on the value of h. Figure 8 shows the evolution to failure of the numerical results of the GVE-DFBM for different values of h. Each data set corresponds to a single simulation for a bundle with $M = 10^7$ standard ($\alpha = 1$) viscoelastic elements and a fixed h. No major differences are expected for other values of α since the results are equivalent in the thermodynamic limit. The strengths are sampled from a Weibull distribution with $m = 1$. The results for the standard DFBM with elastic (instead of viscoelastic) elements are represented as $h = 0$ (circles). Thick light lines represent the analytical solutions found by the approximation to the thermodynamic limit, exhibiting a good agreement with the simulation results. The expression of $\langle\Delta\rangle(f|h)$ is obtained from the ansatz to $\langle\Delta|B\rangle$ introduced in Eq. (18) and considering the analytical relation $f_B(f_\sigma)$ expected for the strength distribution.

Instead of critical failure, the ultimate failure point in the viscoelastic model is reached at $B < 1$, i.e., failure is subcritical. The invariance of $d\Delta/dt$ imposed by the constitutive equation implies a divergence in the activity rate with an exponent that shall match the divergence in $d\Delta/dt$ and the equivalent critical failure for $h = 0$, since the power decomposition of $\langle\Delta\rangle$ for $h > 0$ has a zeroth order (constant) term. Notice that, strictly speaking, due to the divergence in the activity rate, the associated temporal scales introduced by the viscoelasticity can overlap with the driving, even in the thermodynamic limit. This will distort the approximations taken to obtain Eq. (14) and return an avalanche set that may differ from the UC in real systems where the stress evolution is not strictly quasistatic. We don't discuss here the properties of the postpeak activity that may appear as consequence of the splitting of the brittle event in aftershock sequences. We expect this collection of events to fall outside the UC, since the terms ϕ_j in Eq. (12) cannot be neglected any longer.

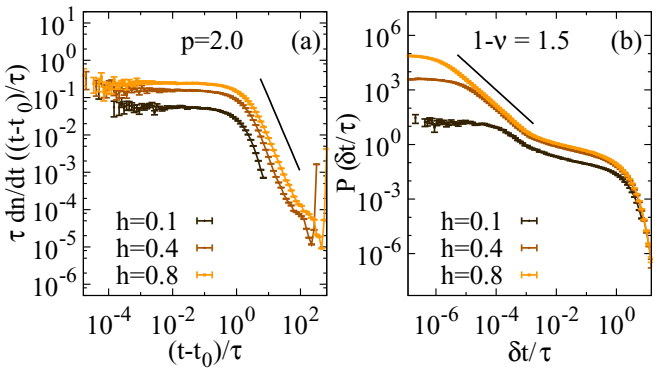

FIG. 9. Temporal correlations in a Zener DFBM (i.e., GVE-DFBM with $\alpha = 1$) for different values of h. (a) Activity rate as function of the time (t_0) since the beginning of the cluster and (b) distribution of waiting times between consecutive events within a cluster. Time is given in units of τ. Straight lines are added as a guide to the eye illustrating the power-law regimes.

D. Presence of power-law temporal correlations

Finally, we can verify that, even for standard viscoelasticity ($\alpha = 1$), the activity rates observed within clusters are compatible with the Omori relation [59] observed in aftershock sequences, reinforcing the link between the presence of aftershocks and the lack of criticality in the presence of transient hardening. Figure 9(b) shows the distribution of waiting times (δt) between events within the same cluster and Fig. 9(a) shows the apparent decay of the activity rate (dn/dt) at time t since the beginning of the cluster at t_0. The simulations correspond to the simple case $\alpha = 1$ and different values of h. For high values of h, the activity exhibits a power-law regime: $dn/dt(\Delta t) \sim \Delta t^{-p}$, with exponent $p \approx 2.0$ for $\Delta t \gtrsim \tau$, resembling the modified Omori relation. The distribution of waiting times (δ) exhibits also a power-law regime: $P(\delta) \sim \delta^{-(1-\nu)}$ superimposed onto an exponential distribution. This exponent $1 - \nu = 1.5$ found in the distribution of waiting times agrees with the relation $1 - \nu = 2 - 1/p$ [59] expected if p is the exponent of the triggering kernel (see Ref. [103]). All the nontrivial temporal profiles tend to vanish for $h \to 0$, as expected in the limit without temporal correlations ($h = 0$) corresponding to the standard DFBM. We expect both exponents p and ν to be sensitive to the driving rate and the fractional exponent α [98] in generalized implementations. The overall distribution of the waiting times and its relation with the triggering rates are particular results of the parametrization, as will be analyzed in future works.

V. DISCUSSION AND CONCLUSIONS

The present paper provides a plausible relation between the macroscopic observation of temporal correlations and lack of critical failure with a microscopical fundamental principle: the presence of a transient hardening mechanism. The generalized viscoelastic democratic fiber bundle model (GVE-DFBM) serves as an example derived from physical principles of a more general category of variations of the DFBM with some mechanism generating transient hardening. In this explicit model, the amount of hardening is quantified and linked to the observable rheological properties of the material.

As a consequence of the transient hardening, the failure point is not critical as one would expect in common conceptual micromechanical models, including the standard DFBM. Instead, the statistical properties of fracture avalanches at the failure point correspond to a subcritical regime with finite correlation lengths and characteristic scales. The activity rate increases up to a divergence compatible with $d\Delta/dt$, which is imposed by the common constitutive equation with the standard DFBM and, thus, is invariant to transient effects under quasistatic driving. One of the most remarkable results is the existence of universal behavior invariant to the parametrization of the model, thus including the standard DFBM. Despite the apparent statistical differences, all the avalanches in any model of fracture compatible with Eq. (14) fall within the same universality class (UC), and are only characterized by the distance to the critical point.

Notice that this universality class, determined by the reduction of the GVE-DFBM to the hitting times of a counting process (14), is not exclusive to the implementation of viscoelasticity, nor transient hardening, nor even fiber bundle models. The universality class will be common to any other mean-field lattice models that can be expressed as Eq. (14) with any alternative temporal evolution of B or different explicit relation $B = g(S_i)$. As a particular case, one might expect that the results discussed in the current work can be extrapolated to the incorporation of generalized viscoelasticity to variations of the DFBM such as continuous damage models. Furthermore, the statistical properties arising from the representation of the avalanche as a hitting time problem (14) are consistent with other MF UCs such as the branching process approach [75] with the same $\tau = 1.5$ and also invariant to dissipation [54]. A deeper relationship, or even the possible equivalence between the two MF models, is yet to be discussed.

Interactions in natural fracture processes are anisotropic and have a finite range generating spatially correlated heterogeneities that can lead to nucleation phenomena, macroscopic defects, or localization bands. In addition, it is difficult to assess how close a system is to failure at the onset of data recording. However, some of the fundamental predictions of this mean-field model can be validated by experimental observations. The stationarity in the statistical properties of AE events recorded during certain experiments [34,89,104] is compatible with the lack of criticality represented in Fig. 8 if the natural internal structure of the material is already close to a critical state at the beginning of the experiment. This condition is supported by the wide range of the scale invariance [34] observed in the stationary energy distribution. Strictly speaking, the amount of AE energy released, and the ASR, will decrease by effect of viscoelasticity due to the energy dissipated by creep. However, in the GVE-DFBM the proportion of dissipated energy is stationary and won't affect the temporal statistics of ASR, which is also a reasonable assumption in more realistic models. In contrast, this model cannot provide an explanation to the increase of activity close to failure observed in the absence of aftershocks [37]. In these experiments, a link is discussed between temporal correlations and local stress fluctuations emerging due to the presence of large heterogeneities. Such experiences might highlight

the role of other processes neglected in this study, such as the weakening of the material due to stress corrosion or the interaction between defects [105,106].

Another phenomenon related to failure that in principle could explain the increase of the energy released is the decrease in the power-law exponent of magnitudes or energies [ϵ in Eq. (1)] sometimes observed close to failure in AE experiments [27,28,33]. Neither conceptual nor numerical micromechanical models of critical failure can reproduce this effect [19]. It has long been suggested that the decrease of the exponent is linked to variations of the stress level [28], a concept that can be related to the distance to failure [19]. Although not explicitly investigated, the same rheological picture presented in this paper might provide an explanation to the change of exponents close to failure. Some of the assumptions considered in the approximation to the thermodynamic limit fail at the yield point, where macroscopic effects appear. In the standard DFBM this macroscopic effect is limited to a single brittle event. In the GVE-DFBM, the transient hardening at the failure point generates a whole triggering tree with specific statistical properties. As mentioned in Sec. IV C, these events cannot be expressed as (14) and, thus, are outside the UC. The identification of such non-UC events as postpeak relaxation might not be possible in finite range interacting systems, where the failure point can be smeared in local interconnected regions due to the material heterogeneity.

This model can set a framework for future experimental studies relating statistical features such as critical failure, ASR, and temporal correlations to driving conditions and internal dynamics. Specifically, the proposed relation between triggering and viscoelasticity can be tested in heterogeneous materials with well parametrized viscoelasticity at the microscale by comparing the triggering rates and criticality with the predictions of the MF model or modifications with complex short-range interactions. Additionally, we have shown in Sec. IV A that in mean-field models of fracture the divergence in $d\Delta/dt$ at failure is determined by the evolution of B as a function of the driving which is difficult to control in some AE experiments [2,107]. Furthermore, it is difficult to clearly discriminate between stick-slip phenomena and microscopic fracture in some AE experiments of fracture [34,37]. We have shown in Sec. IV B that, under the same driving, the exponents related to the divergence of $d\Delta/dt$ are different in the MF approximation of both models. The possible mixture of both kind of processes in some cases, related to dynamic weakening [19], and the variations in the effective driving might explain the variability in the exponent determining the divergence of energy at failure observed in AE experiments [42,43] within the framework of MF theory. This needs to be addressed in future laboratory experiments.

ACKNOWLEDGMENTS

This work was financially supported by the Natural Sciences and Engineering Research Council of Canada (NSERC). We thank G.-Q. Zhang for fruitful discussions.

APPENDIX: NUMERICAL IMPLEMENTATION

To validate the analytical approximations presented in this work, we implement the simplest GVE-DFBM, with $\alpha = 1$, corresponding to the standard Zener element. While the values S_i at which an avalanche is activated are absolutely determined by the constitutive curve and the h parameters, the time intervals between avalanches depend also on the relaxation of the hardening, given by the α values. The selection of $\alpha = 1$ allows a simple implementation since all the history of the process can be simplified. For $\alpha = 1$, the time dependence introduced in the elements ϕ_s can be factorized as $\phi_s(t + dt) = \phi_s(t)\exp(-dt/\tau)$. The interevent times (δt_j) between consecutive fiber breaking $(j, j + 1)$ can be found analytically by imposing a fixed external field σ in Eq. (7) leading to the expression

$$he^{-\delta t_{j/\tau}} = \frac{\Phi h + \frac{\delta F}{(1-F_j)(1-F_{j+1})} + \left(\Phi h - \frac{\delta F}{(1-F_j)}\right)\frac{\delta s}{s_j}}{\Phi + \frac{\delta F}{(1-F_j)(1-F_{j+1})}}, \quad \text{(A1)}$$

where $\Phi := \sum_{t_i<t_j} \phi_i(t_j - t_i)$. Both avalanches and temporal correlations can be obtained from the right-hand term of this equation. When the term is larger than h, the associated interevent time (δt_j) is negative and the next fiber will break instantaneously within the same avalanche. For values between $0, h$ we can associate a triggering interevent time (δt_j) between avalanches. No time can be associated for negative values of the right-hand term, meaning that an increase of the external field σ is required to activate the next breaking. This last situation corresponds to the definition of avalanches in the standard DFBM and, hence, defines independent clusters in the GVE-DFBM. Note that δt has no analytical solution for fractional exponents $0 < \alpha < 1$ and finite driving rates. In such cases, simulations must use the numerical integration of previous history and consider the stress evolution.

[1] J. Li, K. J. Van Vliet, T. Zhu, S. Yip, and S. Suresh, Atomistic mechanisms governing elastic limit and incipient plasticity in crystals, Nature (London) **418**, 307 (2002).

[2] N. Friedman, A. T. Jennings, G. Tsekenis, J.-Y. Kim, M. Tao, J. T. Uhl, J. R. Greer, and K. A. Dahmen, Statistics of Dislocation Slip Avalanches in Nanosized Single Crystals Show Tuned Critical Behavior Predicted by a Simple Mean Field Model, Phys. Rev. Lett. **109**, 095507 (2012).

[3] J. Antonaglia, X. Xie, G. Schwarz, M. Wraith, J. Qiao, Y. Zhang, P. K. Liaw, J. T. Uhl, and K. A. Dahmen, Tuned critical avalanche scaling in bulk metallic glasses, Sci. Rep. **4**, 4382 (2014).

[4] K. M. Salerno and M. O. Robbins, Effect of inertia on sheared disordered solids: Critical scaling of avalanches in two and three dimensions, Phys. Rev. E **88**, 062206 (2013).

[5] R. C. Hidalgo, C. U. Grosse, F. Kun, H. W. Reinhardt, and H. J. Herrmann, Evolution of Percolating Force Chains in

Compressed Granular Media, Phys. Rev. Lett. **89**, 205501 (2002).
[6] D. V. Denisov, K. A. Lőrincz, W. J. Wright, T. C. Hufnagel, A. Nawano, X. Gu, J. T. Uhl, K. A. Dahmen, and P. Schall, Universal slip dynamics in metallic glasses and granular matter–linking frictional weakening with inertial effects, Sci. Rep. **7**, 43376 (2017).
[7] D. Bonamy and E. Bouchaud, Failure of heterogeneous materials: A dynamic phase transition? Phys. Rep. **498**, 1 (2011).
[8] K. Mogi, The influence of the dimensions of specimens on the fracture strength of rocks: Comparison between the strength of rock specimens and that of the earth's crust, Bulletin of the Earthquake Research Institute **40**, 175 (1962).
[9] R. Burridge and L. Knopoff, Model and theoretical seismicity, Bull. Seismol. Soc. Am. **57**, 341 (1967).
[10] Z. Olami, H. J. S. Feder, and K. Christensen, Self-Organized Criticality in a Continuous, Nonconservative Cellular Automaton Modeling Earthquakes, Phys. Rev. Lett. **68**, 1244 (1992).
[11] M. J. Alava, P. K. V. V. Nukala, and S. Zapperi, Statistical models of fracture, Adv. Phys. **55**, 349 (2006).
[12] Y. Ben-Zion, K. A. Dahmen, and J. T. Uhl, A unifying phase diagram for the dynamics of sheared solids and granular materials, Pure Appl. Geophys. **168**, 2221 (2011).
[13] L. Girard, D. Amitrano, and J. Weiss, Failure as a critical phenomenon in a progressive damage model, J. Stat. Mech.: Theor. Exp. (2010) P01013.
[14] A. Shekhawat, S. Zapperi, and J. P. Sethna, From Damage Percolation to Crack Nucleation Through Finite Size Criticality, Phys. Rev. Lett. **110**, 185505 (2013).
[15] L. De Arcangelis, S. Redner, and H. J. Herrmann, A random fuse model for breaking processes, J. Phys. Lett. **46**, 585 (1985).
[16] P. M. Duxbury, P. L. Leath, and P. D. Beale, Breakdown properties of quenched random systems: The random-fuse network, Phys. Rev. B **36**, 367 (1987).
[17] S. Zapperi, P. Ray, H. E. Stanley, and A. Vespignani, First-Order Transition in the Breakdown of Disordered Media, Phys. Rev. Lett. **78**, 1408 (1997).
[18] F. F. Csikor, C. Motz, D. Weygand, M. Zaiser, and S. Zapperi, Dislocation avalanches, strain bursts, and the problem of plastic forming at the micrometer scale, Science **318**, 251 (2007).
[19] D. Amitrano, Variability in the power-law distributions of rupture events, Eur. Phys. J.: Spec. Top. **205**, 199 (2012).
[20] Y. Moreno, J. B. Gomez, and A. F. Pacheco, Fracture and Second-Order Phase Transitions, Phys. Rev. Lett. **85**, 2865 (2000).
[21] F. Kun, S. Zapperi, and H. J. Herrmann, Damage in fiber bundle models, Eur. Phys. J. B **17**, 269 (2000).
[22] J. P. Sethna, K. A. Dahmen, and C. R. Myers, Crackling noise, Nature (London) **410**, 242 (2001).
[23] Y. Ben-Zion, Collective behavior of earthquakes and faults: Continuum-discrete transitions, progressive evolutionary changes, and different dynamic regimes, Rev. Geophys. **46**, RG4006 (2008).
[24] H. Kanamori and E. E. Brodsky, The physics of earthquakes, Rep. Prog. Phys. **67**, 1429 (2004).
[25] C. B. Scruby, An introduction to acoustic emission, J. Phys. E **20**, 946 (1987).
[26] D. Lockner, The role of acoustic emission in the study of rock fracture, Int. J. Rock Mech. Min. Sci. **30**, 883 (1993).
[27] I. G. Main, P. G. Meredith, and C. Jones, A reinterpretation of the precursory seismic *b*-value anomaly from fracture mechanics, Geophys. J. Int. **96**, 131 (1989).
[28] C. H. Scholz, The frequency-magnitude relation of microfracturing in rock and its relation to earthquakes, Bull. Seismol. Soc. Am. **58**, 399 (1968).
[29] P. G. Meredith and B. K. Atkinson, Stress corrosion and acoustic emission during tensile crack propagation in whin sill dolerite and other basic rocks, Geophys. J. Int. **75**, 1 (1983).
[30] J.-C. Anifrani, C. Le Floc'h, D. Sornette, and B. Souillard, Universal log-periodic correction to renormalization group scaling for rupture stress prediction from acoustic emissions, J. de Physique I, EDP Sciences **5**, 631 (1995).
[31] J. Davidsen, S. Stanchits, and G. Dresen, Scaling and Universality in Rock Fracture, Phys. Rev. Lett. **98**, 125502 (2007).
[32] G. Michlmayr, D. Cohen, and D. Or, Sources and characteristics of acoustic emissions from mechanically stressed geologic granular media—a review, Earth-Sci. Rev. **112**, 97 (2012).
[33] T. H. W. Goebel, D. Schorlemmer, T. W. Becker, G. Dresen, and C. G. Sammis, Acoustic emissions document stress changes over many seismic cycles in stick-slip experiments, Geophys. Res. Lett. **40**, 2049 (2013).
[34] J. Baró, Á. Corral, X. Illa, A. Planes, E. K. H. Salje, W. Schranz, D. E. Soto-Parra, and E. Vives, Statistical Similarity Between the Compression of a Porous Material and Earthquakes, Phys. Rev. Lett. **110**, 088702 (2013).
[35] H. V. Ribeiro, L. S. Costa, L. G. A. Alves, P. A. Santoro, S. Picoli, E. K. Lenzi, and R. S. Mendes, Analogies Between the Cracking Noise of Ethanol-Dampened Charcoal and Earthquakes, Phys. Rev. Lett. **115**, 025503 (2015).
[36] L. S. Costa, E. K. Lenzi, R. S. Mendes, and H. V. Ribeiro, Extensive characterization of seismic laws in acoustic emissions of crumpled plastic sheets, Europhys. Lett. **114**, 59002 (2016).
[37] J. Davidsen, G. Kwiatek, E.-M. Charalampidou, T. Goebel, S. Stanchits, M. Rück, and G. Dresen, Triggering Processes in Rock Fracture, Phys. Rev. Lett. **119**, 068501 (2017).
[38] C. U. Grosse and M. Ohtsu, *Acoustic Emission Testing* (Springer-Verlag, Berlin, Heidelberg, 2008).
[39] C. U. Grosse, H. W. Reinhardt, and F. Finck, Signal-based acoustic emission techniques in civil engineering, J. Mater. Civ. Eng. **15**, 274 (2003).
[40] S. C. Jaumé and L. R. Sykes, Evolving towards a critical point: A review of accelerating seismic moment/energy release prior to large and great earthquakes, in *Seismicity Patterns, their Statistical Significance and Physical Meaning* (Springer, Basel AG, 1999), pp. 279–305.
[41] Y. Ben-Zion and V. Lyakhovsky, Accelerated seismic release and related aspects of seismicity patterns on earthquake faults, Earthquake Processes: Physical Modelling, Numerical Simulation and Data Analysis Part II (Springer, Basel AG, 2002), pp. 2385–2412.
[42] H.-h. Zhang, X.-c. Yin, N.-g. Liang, H.-z. Yu, S.-y. Li, Y. C. Wang, C. Yin, V. Kukshenko, N. Tomiline, and S. Elizarov, Acoustic emission experiments of rock failure under load simulating the hypocenter condition, Pure Appl. Geophys. **163**, 2389 (2006).
[43] L. Wang, S. Ma, and L. Ma, Accelerating moment release of acoustic emission during rock deformation in the laboratory, Pure Appl. Geophys. **165**, 181 (2008).

[44] D. Vere-Jones, R. Robinson, and W. Yang, Remarks on the accelerated moment release model: Problems of model formulation, simulation and estimation, Geophys. J. Int. **144**, 517 (2001).
[45] A. Mignan, Retrospective on the accelerating seismic release (ASR) hypothesis: Controversy and new horizons, Tectonophysics **505**, 1 (2011).
[46] R. Robinson, S. Zhou, S. Johnston, and D. Vere-Jones, Precursory accelerating seismic moment release (AMR) in a synthetic seismicity catalog: A preliminary study, Geophys. Res. Lett. **32**, L07309 (2005).
[47] D. Sornette and C. G. Sammis, Complex critical exponents from renormalization group theory of earthquakes: Implications for earthquake predictions, J. Phys. I France **5**, 607 (1995).
[48] D. Amitrano, J. R. Grasso, and G. Senfaute, Seismic precursory patterns before a cliff collapse and critical point phenomena, Geophys. Res. Lett. **32**, L08314 (2005).
[49] K. A. Dahmen, Y. Ben-Zion, and J. T. Uhl, A simple analytic theory for the statistics of avalanches in sheared granular materials, Nat. Phys. **7**, 554 (2011).
[50] J. Vasseur, F. B. Wadsworth, Y. Lavallée, A. F. Bell, I. G. Main, and D. B. Dingwell, Heterogeneity: The key to failure forecasting, Sci. Rep. **5**, 13259 (2015).
[51] J. L. Hardebeck, K. R. Felzer, and A. J. Michael, Improved tests reveal that the accelerating moment release hypothesis is statistically insignificant, J. Geophys. Res. **113**, B08310 (2008).
[52] O. Ramos, Criticality in earthquakes, good or bad for prediction? Tectonophysics **485**, 321 (2010).
[53] A. Vespignani and S. Zapperi, How self-organized criticality works: A unified mean-field picture, Phys. Rev. E **57**, 6345 (1998).
[54] K. Bækgaard Lauritsen, S. Zapperi, and H. E. Stanley, Self-organized branching processes: Avalanche models with dissipation, Phys. Rev. E **54**, 2483 (1996).
[55] A. P. Mehta, K. A. Dahmen, and Y. Ben-Zion, Universal mean moment rate profiles of earthquake ruptures, Phys. Rev. E **73**, 056104 (2006).
[56] E. A. Jagla and A. B. Kolton, A mechanism for spatial and temporal earthquake clustering, J. Geophys. Res. **115**, B05312 (2010).
[57] F. Liakopoulou-Morris, I. G. Main, B. R. Crawford, and B. G. D. Smart, Microseismic properties of a homogeneous sandstone during fault nucleation and frictional sliding, Geophys. J. Int. **119**, 219 (1994).
[58] S. Lennartz-Sassinek, I. G. Main, M. Zaiser, and C. C. Graham, Acceleration and localization of subcritical crack growth in a natural composite material, Phys. Rev. E **90**, 052401 (2014).
[59] T. Utsu, Y. Ogata, and R. S. Matsu'ura, The centenary of the omori formula for a decay law of aftershock activity, J. Phys. Earth **43**, 1 (1995).
[60] I. O. Ojala, I. G. Main, and B. T. Ngwenya, Strain rate and temperature dependence of Omori law scaling constants of AE data: Implications for earthquake foreshock-aftershock sequences, Geophys. Res. Lett. **31**, L24617 (2004).
[61] M. Kloster, A. Hansen, and P. Christian Hemmer, Burst avalanches in solvable models of fibrous materials, Phys. Rev. E **56**, 2615 (1997).
[62] K. Mogi, Earthquakes and fractures, Tectonophysics **5**, 35 (1967).
[63] J. Dieterich, A constitutive law for rate of earthquake production and its application to earthquake clustering, J. Geophys. Res.: Solid Earth **99**, 2601 (1994).
[64] Y. Ben-Zion, and V. Lyakhovsky, Analysis of aftershocks in a lithospheric model with seismogenic zone governed by damage rheology, Geophys. J. Int. **165**, 197 (2006).
[65] S. Hainzl, G. Zöller, and J. Kurths, Similar power laws for foreshock and aftershock sequences in a spring-block model for earthquakes, J. Geophys. Res.: Solid Earth **104**, 7243 (1999).
[66] H. Nakanishi, Earthquake dynamics driven by a viscous fluid, Phys. Rev. A **46**, 4689 (1992).
[67] R. Shcherbakov and D. L. Turcotte, A damage mechanics model for aftershocks, Pure Appl. Geophys. **161**, 2379 (2004).
[68] Y. Kawada and H. Nagahama, Cumulative Benioff strain-release, modified Omori's law and transient behaviour of rocks, Tectonophysics **424**, 157 (2006).
[69] E. A. Jagla, F. P. Landes, and A. Rosso, Viscoelastic Effects in Avalanche Dynamics: A Key to Earthquake Statistics, Phys. Rev. Lett. **112**, 174301 (2014).
[70] E. Lippiello, F. Giacco, W. Marzocchi, C. Godano, and L. De Arcangelis, Mechanical origin of aftershocks, Sci. Rep. **5**, 15560 (2015).
[71] Y. Ogata, Statistical models for earthquake occurrences and residual analysis for point processes, J. Am. Stat. Assoc. **83**, 9 (1988).
[72] C. Gu, A. Y. Schumann, M. Baiesi, and J. Davidsen, Triggering cascades and statistical properties of aftershocks, J. Geophys. Res.: Solid Earth **118**, 4278 (2013).
[73] I. Zaliapin and Y. Ben-Zion, Earthquake clusters in southern california i: Identification and stability, J. Geophys. Res.: Solid Earth **118**, 2847 (2013).
[74] J. Baró and J. Davidsen, Are triggering rates of labquakes universal? Inferring triggering rates from incomplete information, Eur. Phys. J.: Spec. Top. **226**, 3211 (2017).
[75] S. Zapperi, K. B. Lauritsen, and H. E. Stanley, Self-Organized Branching Processes: Mean-Field Theory for Avalanches, Phys. Rev. Lett. **75**, 4071 (1995).
[76] S. Pradhan and B. K. Chakrabarti, Precursors of catastrophe in the Bak-Tang-Wiesenfeld, Manna, and random-fiber-bundle models of failure, Phys. Rev. E **65**, 016113 (2001).
[77] F. Kun, F. Raischel, R. C. Hidalgo, and H. J. Herrmann, Extensions of fibre bundle models, in *Modelling Critical and Catastrophic Phenomena in Geoscience* (Springer-Verlag, Berlin, Heidelberg, 2006), pp. 57–92.
[78] R. C. Hidalgo, F. Kun, and H. J. Herrmann, Bursts in a fiber bundle model with continuous damage, Phys. Rev. E **64**, 066122 (2001).
[79] Z. Halász and F. Kun, Fiber bundle model with stick-slip dynamics, Phys. Rev. E **80**, 027102 (2009).
[80] S. Hergarten and H. J. Neugebauer, Foreshocks and Aftershocks in the Olami-Feder-Christensen Model, Phys. Rev. Lett. **88**, 238501 (2002).
[81] S. Hergarten and R. Krenn, Synchronization and desynchronization in the Olami-Feder-Christensen earthquake model and potential implications for real seismicity, Nonlin. Processes Geophys. **18**, 635 (2011).
[82] M. Paczuski, S. Boettcher, and M. Baiesi, Interoccurrence Times in the Bak-Tang-Wiesenfeld Sandpile Model: A Comparison with the Observed Statistics of Solar Flares, Phys. Rev. Lett. **95**, 181102 (2005).

[83] A. Deluca, N. R. Moloney, and Á. Corral, Data-driven prediction of thresholded time series of rainfall and self-organized criticality models, Phys. Rev. E **91**, 052808 (2015).

[84] S. Janićević, L. Laurson, K. Jørgen Måløy, S. Santucci, and M. J. Alava, Interevent Correlations from Avalanches Hiding Below the Detection Threshold, Phys. Rev. Lett. **117**, 230601 (2016).

[85] H. Benioff, Earthquakes and rock creep: (Part I: Creep characteristics of rocks and the origin of aftershocks), Bull. Seismol. Soc. Am. **41**, 31 (1951).

[86] V. B. Smirnov and A. V. Ponomarev, Seismic regime relaxation properties from in situ and laboratory data, Izv., Acad. Sci., USSR, Phys. Solid Earth (Engl. Transl.) **40**, 807 (2004).

[87] J. Davidsen and M. Baiesi, Self-similar aftershock rates, Phys. Rev. E **94**, 022314 (2016).

[88] T. Hirata, Omori's power law aftershock sequences of microfracturing in rock fracture experiment, J. Geophys. Res.: Solid Earth **92**, 6215 (1987).

[89] G. F. Nataf, P. O. Castillo-Villa, J. Baró, X. Illa, E. Vives, A. Planes, and E. K. H. Salje, Avalanches in compressed porous sio_2-based materials, Phys. Rev. E **90**, 022405 (2014).

[90] W. G. Glöckle and Th. F. Nonnenmacher, Fractional relaxation and the time-temperature superposition principle, Rheol. Acta **33**, 337 (1994).

[91] N. Heymans and J.-C. Bauwens, Fractal rheological models and fractional differential equations for viscoelastic behavior, Rheol. Acta **33**, 210 (1994).

[92] S. Hellinckx, N. Heymans, and J.-C. Bauwens, Analytical and fractal descriptions of non-linear mechanical behavior of polymers, J. Non-Cryst. Solids **172**, 1058 (1994).

[93] H. Schiessel, R. Metzler, A. Blumen, and T. F. Nonnenmacher, Generalized viscoelastic models: Their fractional equations with solutions, J. Phys. A **28**, 6567 (1995).

[94] C. H. R. Friedrich, Relaxation and retardation functions of the Maxwell model with fractional derivatives, Rheol. Acta **30**, 151 (1991).

[95] G. W. Scott Blair, The role of psychophysics in rheology, J. Colloid Sci. **2**, 21 (1947).

[96] A. Jaishankar and G. H. McKinley, Power-law rheology in the bulk and at the interface: Quasi-properties and fractional constitutive equations, Proc. R. Soc. A **469**, 20120284 (2013).

[97] F. Mainardi and G. Spada, Creep, relaxation and viscosity properties for basic fractional models in rheology, Eur. Phys. J.: Spec. Top. **193**, 133 (2011).

[98] X. Zhang and R. Shcherbakov, Power-law rheology controls aftershock triggering and decay, Sci. Rep. **6**, 36668 (2016).

[99] M. Baiesi and M. Paczuski, Scale-free networks of earthquakes and aftershocks, Phys. Rev. E **69**, 066106 (2004).

[100] S. Hainzl, A. Christophersen, D. Rhoades, and D. Harte, Statistical estimation of the duration of aftershock sequences, Geophys. J. Int. **205**, 1180 (2016).

[101] D. L. Turcotte, J. R. Holliday, and J. B. Rundle, BASS, an alternative to ETAS, Geophys. Res. Lett. **34**, L12303 (2007).

[102] K. A. Dahmen, Mean field theory of slip statistics, In *Avalanches in Functional Materials and Geophysics* (Springer International Publishing, Cham, 2017), pp. 19–30.

[103] A. Corral, Local distributions and rate fluctuations in a unified scaling law for earthquakes, Phys. Rev. E **68**, 035102 (2003).

[104] P. O. Castillo-Villa, J. Baró, A. Planes, E. K. H. Salje, P. Sellappan, W. M. Kriven, and E. Vives, Crackling noise during failure of alumina under compression: The effect of porosity, J. Phys.: Condens. Matter **25**, 292202 (2013).

[105] M. Kachanov, Elastic solids with many cracks and related problems, Adv. Appl. Mech. **30**, 259 (1993).

[106] T. Yamashita and L. Knopoff, Models of aftershock occurrence, Geophys. J. Int. **91**, 13 (1987).

[107] R. Maaß, M. Wraith, J. T. Uhl, J. R. Greer, and K. A. Dahmen, Slip statistics of dislocation avalanches under different loading modes, Phys. Rev. E **91**, 042403 (2015).